

Role of Van Hove singularity in high-temperature superconductors: Mean field

D. M. News, P. C. Pattnaik, and C. C. Tsuei

IBM Research Division, Thomas J. Watson Research Center, P. O. Box 218, Yorktown Heights, New York 10598

(Received 25 May 1990; revised manuscript received 7 August 1990)

Realistic $U = \infty$ models, for oxide superconductors are solved in slave-boson mean-field approximation. A successful understanding is achieved of the paramagnetic susceptibility and specific heat, the energy dispersion seen in photoemission, the shape and topology of the Fermi surface, the relative weights of copper and oxygen both in NMR and photoemission spectroscopies and the observed energy gaps in the p - and n -type materials. The Fermi level is found to lie very close to the nearly logarithmic van Hove singularity in the density of states over a substantial range of doping. This makes it possible without large Fermi-liquid parameters to reconcile the light mass found in photoemission experiments with the high density of states deduced from thermodynamic data. Further important consequences for the behavior of the imaginary part of the self-energy and for pairing mechanisms are outlined.

I. INTRODUCTION

The high-temperature superconductors pose some deep questions regarding the nature of strongly correlated systems in two dimensions. Following the original suggestion of Anderson,¹ spectroscopic^{2,3} and theoretical⁴ studies have shown the existence of a large intra-atomic Coulomb repulsion U on the Cu atom of 5–10 eV, larger than the hopping matrix elements of order 1 eV.

Experiments show surprising effects apparently arising from the strong coupling, such as scaling of Hall coefficient with the doping x_h (not the Luttinger Fermi-surface volume $1+x_h$), scaling of resistivity with temperature, and inverse quasiparticle lifetime in infrared⁵ and photoemission⁶ scaling with energy. These experimental results contrast with the simplest Fermi-liquid picture,^{7,8} which gives resistivity going as $T^2 \ln T$ and inverse lifetime going as $\epsilon^2 \ln \epsilon$.

However, the Hall coefficient results cannot be naively interpreted in terms of a carrier gas containing x_h particles,^{9,10} because angle-resolved photoemission⁶ measurements suggest that there is a Luttinger Fermi surface, containing $1+x_h$ holes. This result combined with thermodynamic data such as the existence of a temperature-independent susceptibility and a constant χ/γ ratio would tend, on the contrary, to suggest a straightforward Fermi liquid picture of the high- T_c materials. Indeed a more recent look at the resistivity behaviors show that the Nd-Ce-Cu-O system and several low- T_c hole-doped superconductors show more nearly quadratic temperature dependence.¹¹ Attempts to reconcile these Fermi-liquid-like results with the nonconventional transport and lifetime data described in the foregoing have led to marginal Fermi-liquid¹² and novel gauge-theory¹³ scenarios.

The mechanism of superconductivity, if it is to be thought of in terms of conventional pairing, seems unlikely to proceed entirely from phonons, without invoking some anomalous electronic contribution, in view of the absence of any structure at $2\Delta + \omega_{ph}$ in the ir conductivity below T_c ,⁵ as well as the low isotope shift. There is also no structure at $2\Delta + \omega_{mag}$, where ω_{mag} is of the order of the dd exchange energy 130 meV. Hence if it is “conventional,” superconductivity seems to proceed from ex-

citations above 0.4 eV,⁵ essentially outside the retarded regime.

Additional constraints on the mechanism¹⁴ of superconductivity are becoming available from Monte Carlo simulations on simplified models such as the Hubbard¹⁵ and Emery¹⁵ models. These models have been found not to show any sign of s -wave superconductivity. This is consistent with the absence of magnetic satellite structure in the low-temperature ir conductivity, because these models show antiferromagnetic peaks in the spin-spin correlation function, and if magnetic excitations were mediating s -wave pairing these models might be expected to be s -wave superconductors. These negative results suggest that the source of the pairing interaction must be looked for in additional interactions in the model, e.g., such factors as the direct oxygen-oxygen hopping,¹⁶ the copper-oxygen Coulomb interaction,¹⁷ or quadrupole coupling¹⁸ leading to virtual excitation of holes into the z^2 orbital. A scenario is emerging where the importance of such details of the model requires us to establish a quantitative picture of the high T_c 's as far as possible. This requirement has motivated the present paper.

The present work is based on the apparent closeness of the systems to Fermi liquids. A Fermi-liquid model is employed that treats the strong coupling via slave-boson mean-field theory, in which respect we extend and interpret earlier work.^{16,19} Bearing in mind the emphasis on secondary interactions, we use the Anderson lattice (“extended Hubbard”) model in a form derived without further modification from the band-structure parametrization work of the Naval Research Laboratory group.^{19,20} Despite the claims of the t - J model, founded on single-hole calculations,²¹ we feel that at finite doping, and in view of the absence of Monte Carlo evidence for s -wave pairing in the t - J model so far, we should go at least to the full Anderson-lattice model.

Here we calculate some thermodynamic and spectroscopic properties within our realistic slave-boson mean-field theory. The main surprise is that the Fermi level lies very close to the Van Hove singularity in the density of states, which consists of a logarithmic divergence in the case of isolated CuO_2 layers. The Van Hove singularity is not correlated with the half-filling point, as in the Hub-

bard model, but occurs at a finite doping in the 15–35 % range, depending on long-range interactions in the model, and is not necessarily correlated with magnetism. The high density of states at the Fermi level, associated with nearness to the singularity, is shown to be consistent with the thermodynamic data on the high- T_c materials. This high density of states occurs without requiring an especially large mass, consistent with the angle-resolved photoemission data.

II. MODELS AND MEAN FIELD

The generic features of the model are illustrated in Fig. 1. The oxygen $2p$ levels (not pure but hybridized with the Cu $4s$ and other states) form a band about 4 eV wide in the absence of hybridization with the Cu d states. The Cu atom has a hole ionization level (d^9 - d^{10} level) at E_1 , at energy Δ (=oxide gap, charge-transfer gap) below the bottom of the oxygen hole band; in addition it has a hole affinity level E_2 at U , the intra- d -orbital Coulomb interaction, above E_1 . These are the exact eigenstates in the absence of mixing \mathcal{H}_{mix} between the oxygen and copper orbitals, denoted by V in Fig. 1, or intersite d - d interaction. In this paper we use slave-boson mean-field theory to approximately project out the $E_2(d^8)$ state when V is switched on.

The specific models we are working with are reasonably standard but a little more inclusive than in many current calculations. These differences now seem likely to be important or even essential, to getting a sensible picture of high-temperature superconductors. To get a feeling for the real situation, we consider two models, a very minimal model, applicable only to the CuO_2 planes, which originated in the $\text{Bi}_2\text{Sr}_2\text{CaCuO}_8$ with $n=2$ (2:2:1:2) material, and a highly complete model of the full

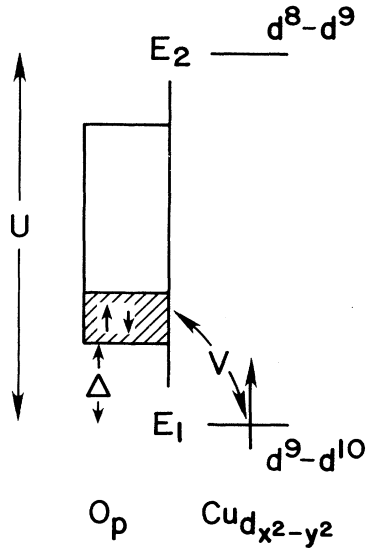


FIG. 1. Energy level diagram for CuO_2 planes, prior to switching on \mathcal{H}_{mix} denoted by V . Left: energy bands of oxygen $2p\sigma$ levels. Shaded area illustrates doped holes. Right: hole ionization energy E_1 , and hole affinity level E_2 of copper $d_{x^2-y^2}$ orbital. Hole notation.

La_2CuO_4 (2:1:4) material. We avoid modeling the $\text{YBa}_2\text{Cu}_3\text{O}_{7-x}$ (1:2:3) material because of the complication introduced by the chains.

The 2:2:1:2 model is then a model of the CuO_2 planar sigma bonds in the $p_x, p_y, d_{x^2-y^2}$ basis set. The matrix elements are those obtained in the tight binding fit of De Weert *et al.*²⁰ to the band structure of the 2:2:1:2 material. This is a very minimal fit, but it does include second-nearest-neighbor oxygen-oxygen interactions.

The Hamiltonian may be written

$$\mathcal{H}_0 = \sum_{p,q,\sigma} t_{pq} (c_{p\sigma}^\dagger c_{q\sigma} + \text{H.c.}), \quad (1a)$$

$$\mathcal{H}_1 = E_1 \sum_{i,\sigma} D_{i\sigma}^\dagger D_{i\sigma} + \sum_{i,j,\sigma} t_{ij} D_{i\sigma}^\dagger D_{j\sigma}, \quad (1b)$$

$$\mathcal{H}_{\text{mix}} = \sum_{i,p,\sigma} t_{ip} (D_{i\sigma}^\dagger c_{p\sigma} + \text{H.c.}). \quad (1c)$$

Here p describes the oxygen sigma $2p$ orbitals (p_x or p_y) at site p , while i describes the $d_{x^2-y^2}$ orbital at site i . We take the oxygen energy level as zero. The matrix elements in (1) are derived from the canonical overlap integrals²⁰ listed in Table I. In (1), Eq. (1a) describes the band structure of the oxygen $2p$ orbitals alone, which has a band width of order 4 eV. The effect of coupling in the copper orbitals is linked to taking into account the Coulomb interaction, which is discussed below.

The 2:1:4 model is the 32-band model employed earlier,¹⁹ which is a complete parametrization of the 2:1:4 band structure.²⁰ This model incorporates all the Cu $3d$ and oxygen $2p$ orbitals, together with the Cu $4s$ and $4p$, and the La $5d$ orbitals. Its Hamiltonian may be written

$$\mathcal{H}_0 = \sum_{p,\sigma} \epsilon_p c_{p\sigma}^\dagger c_{p\sigma} + \sum_{p,q,\sigma} t_{pq} (c_{p\sigma}^\dagger c_{q\sigma} + \text{H.c.}), \quad (2a)$$

$$\mathcal{H}_1 = E_1 \sum_{i,\alpha,\sigma} D_{i\alpha\sigma}^\dagger D_{i\alpha\sigma} + \sum_{i,j,\alpha,\beta,\sigma} t_{ij\alpha\beta} D_{i\alpha\sigma}^\dagger D_{j\beta\sigma}, \quad (2b)$$

$$\mathcal{H}_{\text{mix}} = \sum_{i,\alpha,p,\sigma} t_{i\alpha p} (D_{i\alpha\sigma}^\dagger c_{p\sigma} + \text{H.c.}). \quad (2c)$$

Here $i\alpha$ denotes the Cu $3d$ orbitals of e_g symmetry, and p denotes all the other states in the basis set. The canonical matrix elements in the model are listed in Ref. 20.

As already pointed out, the most important Coulomb interaction in these systems is usually considered to be the intrasite Cu $3d$ Coulomb interaction U , which in this paper is taken to be infinite. Implementation of the restriction that double occupation of Cu $3d$ be forbidden can be done with slave bosons. In (1), the ansatz

$$D_{i\sigma} = b_i^\dagger d_{i\sigma}, \quad (3a)$$

where b_i is a boson and $d_{i\sigma}$ a fermion, together with the constraint

$$\hat{Q}_i = \sum_{\sigma} d_{i\sigma}^\dagger d_{i\sigma} + b_i^\dagger b_i = 1, \quad (3b)$$

leads to the Hamiltonian which, when the constraint is taken into account via a Lagrange multiplier, becomes^{16,19,22,23}

$$\mathcal{H}' = \mathcal{H}_0 + E_1 \sum_{i,\sigma} d_{i\sigma}^\dagger d_{i\sigma} + \sum_{i,j,\sigma} t_{ij} b_i b_j^\dagger d_{i\sigma}^\dagger d_{j\sigma} + \sum_{i,p,\sigma} t_{ip} (b_i d_{i\sigma}^\dagger c_{p\sigma} + \text{H.c.}) + \lambda \sum_i (\hat{Q}_i - 1). \quad (4)$$

In the mean field approximation, wherein b_i is replaced by $\langle b \rangle$, (4) becomes the mean-field Hamiltonian

$$\mathcal{H}_{\text{MF}} = \mathcal{H}_0 + \varepsilon_d \sum_{i,\sigma} d_{i\sigma}^\dagger d_{i\sigma} + \langle b \rangle^2 \sum_{i,j,\sigma} t_{ij} d_{i\sigma}^\dagger d_{j\sigma} + \langle b \rangle \sum_{i,p,\sigma} t_{ip} (d_{i\sigma}^\dagger c_{p\sigma} + \text{H.c.}) + (\varepsilon_d - E_1) \sum_i (\langle b \rangle^2 - 1), \quad (5)$$

where $\varepsilon_d = E_1 + \lambda$. The quantities ε_d and λ are found by minimizing $\langle \mathcal{H}_{\text{MF}} \rangle$.

In the case of the 2:1:4 model, we assume that the t_{2g} orbitals will lie too deep to be occupied by holes. Then the assumption of infinite U requires that we allow only d^9 and d^{10} configurations in the e_g subspace, so (3)–(5) generalize to

$$D_{i\alpha\sigma} = b_i^\dagger d_{i\alpha\sigma}, \quad (6a)$$

$$\hat{Q}_i = \sum_{\alpha,\sigma} d_{i\alpha\sigma}^\dagger d_{i\alpha\sigma} + b_i^\dagger b_i = 1, \quad (6b)$$

$$\mathcal{H}' = \mathcal{H}_0 + E_1 \sum_{i,\alpha,\sigma} d_{i\alpha\sigma}^\dagger d_{i\alpha\sigma} + \sum_{i,j,\alpha,\beta,\sigma} t_{ij\alpha\beta} b_i b_j^\dagger d_{i\alpha\sigma}^\dagger d_{j\beta\sigma} + \sum_{i,p,\alpha,\sigma} t_{iap} (b_i d_{i\alpha\sigma}^\dagger c_{p\sigma} + \text{H.c.}) + \lambda \sum_i (\hat{Q}_i - 1), \quad (7)$$

$$\mathcal{H}_{\text{MF}} = \mathcal{H}_0 + \varepsilon_d \sum_{i,\alpha,\sigma} d_{i\alpha\sigma}^\dagger d_{i\alpha\sigma} + \langle b \rangle^2 \sum_{i,j,\alpha,\beta,\sigma} t_{ij\alpha\beta} d_{i\alpha\sigma}^\dagger d_{j\beta\sigma} + \langle b \rangle \sum_{i,\alpha,p,\sigma} t_{iap} (d_{i\alpha\sigma}^\dagger c_{p\sigma} + \text{H.c.}) + (\varepsilon_d - E_1) \sum_i (\langle b \rangle^2 - 1). \quad (8)$$

The method we use starts from the mean-field Hamiltonian (5) or (8) with assumed values of ε_d and $\langle b \rangle$. A band structure is generated from which the densities of states, etc., are calculated by the triangle or tetrahedron methods. The triangle method is an adaptation to purely two-dimensional models of the tetrahedron method. Then ε_d and $\langle b \rangle$ may be iterated to self-consistency.

The only free parameter in the method is the copper-oxygen energy difference E_1 , which can be thought of as the charge-transfer gap measured from the center of the oxygen band. This parameter sets the overall energy scale of the CuO_2 antibonding band, in which the Fermi level lies. We set E_1 so as to get, as far as possible, similar results in the two models, and fit the Pauli susceptibility of the 2:1:4 material.

In Table II we compare the mean-field solutions to the 2:1:4 and 2:2:1:2 models. The value of E_1 is defined in the 2:1:4 model relative to the planar oxygen levels. We usually work in a framework of holes, so the energy axis has the opposite sense to the conventional one, and E_1 is negative. This represents the fact that there is an energy cost to transfer a hole from the Cu to the planar oxygen orbitals. We chose $E_1 = -5.0$ eV as a reasonable value. This value implies that the lowest $d^9 \rightarrow d^{10}$ excitation (“oxide gap,” charge-transfer gap) is about 3 eV.

The two models are seen to be reasonably similar, especially if the 2:1:4 at doping $x_h = 0.1$ is compared with the 2:2:1:2 at a higher doping such as 0.25. Further, close

similarity will be seen on comparison of Figs. 3(a), 3(b), 4(a), and 4(b) below. The density of states (DOS) is, however, so narrowly peaked in the 2:2:1:2 model that a very high DOS is only achieved in a narrow range of doping. In the 32-band (2:1:4) model, the overlap of many bands makes the lower band edges difficult to determine for purposes of comparison.

Most importantly, the calculations of Table II suggest that the simple three-band 2:2:1:2 model can to a considerable extent duplicate the properties of a highly realistic model such as the 2:1:4 model.

In the following, we calculate some of the properties of the mean-field Hamiltonians (5) and (8) and compare with experimental data.

III. RESULTS

Let us start this section by noting some striking features of the thermodynamic data on various high- T_c materials. In Table II we have analyzed specific heat and susceptibility data in a manner that is conventional in the heavy-fermion field. The specific heat has been derived by a crude but consistent BCS analysis of the specific-heat jump, involving the conventional factor 1.43 be-

TABLE I. Parameters in 2:2:1:2 model.

Integral	eV
Cu-O(1) ($dp\sigma$)	-1.29
Cu-Cu ($dd\sigma$)	0.037
Cu-Cu ($dd\delta$)	-0.170
O(1)-O(1) ($pp\sigma$)	0.894
O(1)-O(1) ($pp\pi$)	-0.162
O(1)-O(1) (NNN) ($pp\sigma$)	0.087
O(1)-O(1) (NNN) ($pp\pi$)	0.024

TABLE II. Mean-field solutions to 2:2:1:2 and 2:1:4 models.

	2:2:1:2	2:2:1:2	2:1:4
x_h	0.1	0.25	0.1
$\langle b \rangle^2$	0.23	0.21	0.20
E_1	-5.0	-5.0	-4.92
μ	-2.8	-2.2	-1.9
ε_d	-2.3	-1.7	-1.4
ρ_F	2.5	2.8	5.1
ε_F	0.45	0.46	
FS	h	h	h
Band 1 edge	-3.6	-3.3	-2.8
Band 2 edge	-2.3	-1.8	
Band 3 edge	-0.55	-0.35	

tween the jump and γT_c . The analysis of the data on the uniform magnetic susceptibility is a little more lengthy. The diamagnetic core corrections must first be made, then we also made an allowance for the Van Vleck susceptibility, taking in all cases the value of Mehran *et al.*²⁴

We then converted the values deduced from the data for the electronic specific heat γ and the Pauli susceptibility χ_P into density of states at the Fermi level (including spin) ρ_F , using the mean-field relationships:

$$\chi_P = \mu_B^2 \rho_F, \quad (9a)$$

$$\gamma = (\pi^2/3) \rho_F. \quad (9b)$$

The result of these manipulations on the data is seen in Table III, in which the DOS per Cu atom derived from the susceptibility and specific-heat data are compared. It is seen that the DOS values derived by the two methods are remarkably close. We already noticed this agreement at an early stage in the high- T_c field in the case of the 2:1:4 material.¹⁹ In fact, the agreement is closer in some cases than the accuracy of the reduction procedures and the data themselves allow, and is partly fortuitous. Nevertheless, the pattern of Table III is typical of what is found in the heavy Fermion field, and strongly supports Fermi-liquid behavior. Similar observations have been made by Millis and by Crowe *et al.*²⁶

The second remarkable fact about Table III is that the values of the DOS are surprisingly high. Shortly we shall consider how this fact may be reconciled with the relatively light mass seen in direct observation of the energy dispersion.

There could be artifacts responsible for part of the high value of DOS. One is obviously that the Pauli susceptibility could well be enhanced in magnetic systems like these. This would lead to the experimental DOS from χ_P being reduced relative to that in Table III by the enhancement factor. Secondly, we know that T_c is reduced below the BCS value, an effect that could be argued to increase the specific-heat jump, and hence to an overestimate of the DOS derived from the jump in Table III. In this paper we shall ignore these hard to quantify factors; a reduction in the values in Table III by 30–40% or so would not much affect the conclusions of this paper.

In Fig. 2 we illustrate the DOS as a function of doping for our two models, compared with 2:1:4 and 2:2:1:2 data from Table III. The 2:1:4 model, as far as has been calculated, rather accurately fits the susceptibility data. Note that our disposable parameter E_1 was chosen for this fit. The 2:1:4 model breaks down at $x > 15\%$, due to closure of the gap between ϵ_F and the bottom of the oxygen

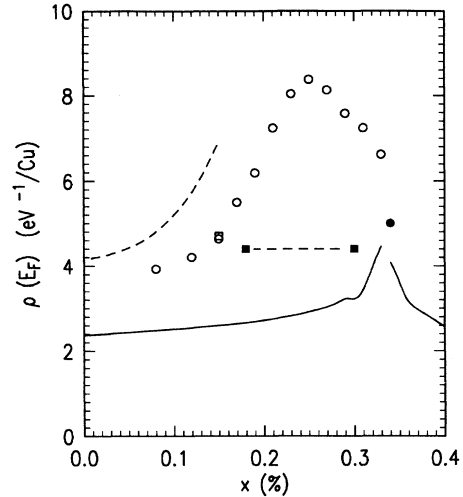


FIG. 2. Open and solid circles: paramagnetic χ of 214²⁹ and 2212³⁰ materials expressed as DOS using (9a), vs hole concentration x ; open and solid squares: DOS from specific-heat jump data, derived as per text, for 2:1:4,²⁷ and 2:2:1:2.²⁶ The doping of the Ref. 26 sample not stated, a wide error bar assumed. Dashed curve: mean-field approximation for 2:1:4 material as per Ref. 19; full curve: mean-field theory for 2:2:1:2 in model of Table I.

(hole) band.³¹ The success of this model in getting the high observed DOS values originates in its ability to accurately reproduce the Van Hove singularity in the DOS, which ϵ_F scans through in the experimental doping range. The cruder 2:2:1:2 model gets a high DOS only over a narrow range of doping, and due to uncertainties in the actual 2:2:1:2 doping it remains unclear whether the simple 2:2:1:2 model can fully explain the observed χ_P and C_V values.

Next we illustrate the band structure of the models and compare directly with angle-resolved photoemission data.⁶ In Fig. 3(a), we illustrate the band structure of the 2:1:4 model at 10% doping. This curve was derived as long ago as early 1988 following parametrization of the 2:1:4 in Ref. 20 and fitting of E_1 to susceptibility data. It is seen that this old calculation rather well predicted the photoemission measurements of Olson *et al.*,⁶ as we already pointed out in Ref. 32. In Fig. 3(b) we show the same comparison for the 2:2:1:2 model, remembering that the measurements were actually done on this material. There is also seen to be a reasonable fit.

The effective mass in, for example the theoretical curve of Fig. 3(b) is not especially large, 3.3 electron masses. A 2D electron gas with this mass would have a DOS of $\rho_F = 2.0 \text{ eV}^{-1}$. This is markedly lower than the values in Table III, which go up to 6 eV^{-1} .

Notice that along the other direction plotted, in which photoemission data has not been shown, $\Gamma-Z$, the bands lie very close to the Fermi level. This effect is in fact responsible for the high thermodynamic density of states deduced in Fig. 2 from the same calculation that led to these band structures. In other words, the fact that the bands are highly non-free-electron-like and track the Fermi level in directions other than Γ to X leads to high

TABLE III. DOS derived from specific-heat and susceptibility data.

	eV^{-1} DOS- ΔC_v	eV^{-1} DOS- χ_P
1:2:3	6.4 (Ref. 25)	6.3 (Ref. 28)
2:2:2:3 ($n=3$)	5.6 (Ref. 26)	5.6 (Ref. 26)
2:1:4	4.7 (Ref. 27)	4.6 (Ref. 29)
2:2:1:2 ($n=2$)	4.4 (Ref. 26)	5.0 (Ref. 30)

DOS despite the modest mass. This is another way of saying that the Fermi level in these systems seems to lie close to the Van Hove singularity, which is almost a logarithmic singularity in these nearly two-dimensional systems.

In Figs. 4(a) and 4(b) we illustrate the Fermi surface found in the foregoing calculations. First point to notice, of which many people seem unaware, is that for the 2:1:4 model at 10% doping and for the 2:2:1:2 model at 30% and below, the Fermi surface is hole-type. It is often thought, by false analogy with the Hubbard model, that the Fermi surface must be electron-type below half-filling and perfectly nested at half filling. The situation in realistic mean-field models is in fact that the Fermi surface

changes type at some finite doping, for the 2:2:1:2 model at $\frac{1}{3}$ doping, a value that depends on the longer-range interactions in the model and that can be tuned over a wide range.

The crossover, which in the 2:2:1:2 model is at approximately 0.33 doping, corresponds [see Fig. 4(b), middle panel] to the Fermi level lying at the van Hove singularities located on the zone edges at $(\pi, \pi/2)$ and $(\pi/2, \pi)$. At this point the hole and electron regions do not map onto one another: because of the nonzero doping, their areas are unequal, and the Fermi edge must be curved. There is no nesting.

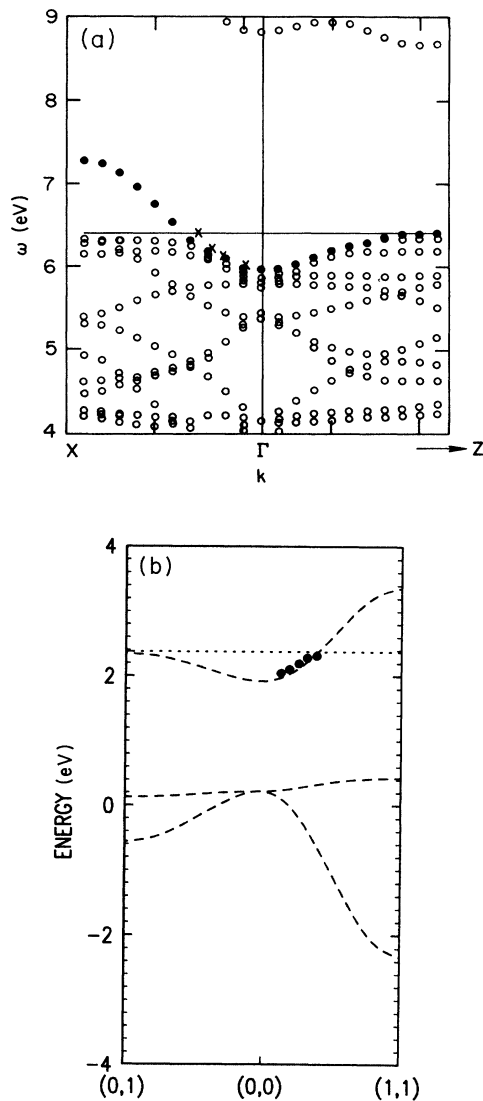


FIG. 3. (a) Open and solid circles: band structure calculated according to Ref. 19 at $x=0.1$ for 2:1:4 material; crosses: photoemission data of Ref. 6. (b) Band structure for 2:2:1:2 model of Table I, $x=0.2$, compared with more recent version of same photoemission data. Conventional electron notation is used in these figures.

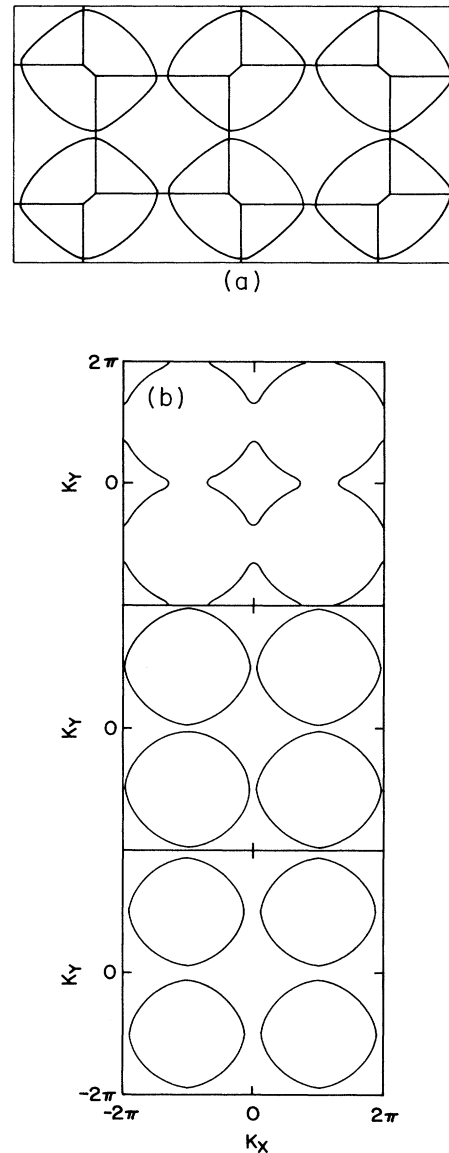


FIG. 4. (a) Fermi surface of 2:1:4 material in mean field calculation of Ref. 19, $x=0.1$. Closed regions are hole-type. (b) Fermi surface of 2:2:1:2 model in mean field calculation based on Table I. Bottom panel, $x=0.25$, closed regions hole-type, middle panel, $x=0.30$, closed regions hole-type, top panel, $x=0.55$, closed regions electron-type.

Another view of what happens as the doping is increased is seen in the series of DOS plots in Fig. 5. First of all there is a uniform shift up in (hole-type) energy as doping is increased. This is a kind of hole-hole repulsion effect. It is likely that the repulsion effect is partly canceled by the doping centers,³¹ which exert an attraction on the holes. In fact, the Friedel sum rule assures that the added hole charge density remains localized around the doping centers.

More importantly, we see that there is not a uniform shift of the whole band, but rather as doping increases the nearly half-filled "Hubbard resonance" moves up relative to the oxygenlike environment, allowing the extra holes to be taken up by the low-DOS oxygenlike states at the bottom of the band. This effect is reminiscent of a heavy-fermion resonance, which floats up to follow the Fermi level if more electrons are added to the valence band. At the same time we see how the Fermi level is not completely pinned at the resonance center but slowly crosses through the Van Hove singularity, allowing the switch in Fermi surface from holelike to electronlike illustrated in Fig. 4(b).

In Fig. 6 we illustrate various projected densities of states. The $3d$ DOS (dotted curve) is seen to be fractionally the greatest near the top of the band (bottom of band in conventional representation). This high occupation is continued into the near edge of the oxygen band (not shown). On the other hand the oxygen component (dashed line) is greatest near the bottom of the band (above the Fermi level in conventional notation). This is where the extra holes go upon further doping, when, as just pointed out, the Van Hove singularity marking the d resonance moves up. Thus the way to think about the mean-field band structure is as a $3d$ resonance in an oxygen background, the resonance being trapped close to the Fermi level, where most of the d DOS is located.

The weights of $3d$ and $2p$ character states are further illustrated in the dot-dashed curve in Figs. 6 and 7. The Fig. 6 curve illustrates $\langle b \rangle^2$ times the $3d$ DOS. This is the quantity that actually enters into the d weight in photoemission. The weights now no longer add to one, the

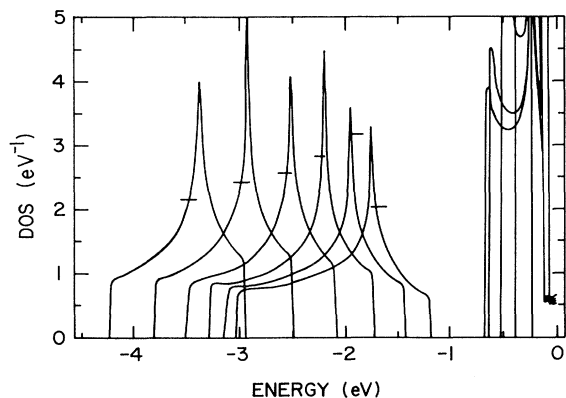


FIG. 5. Mean field DOS of 2:2:1:2 model (Table I) for a range of dopings between $x = -0.05$ and $x = 0.45$ (indicated in figure). Horizontal bars indicate DOS at Fermi level. Hole notation.

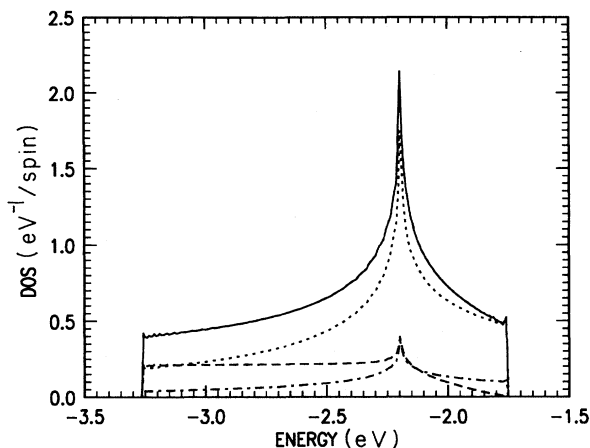


Fig. 6. Mean field DOS and projected densities of states of 2:2:1:2 model (Table I) at $x = 0.25$, hole notation. Solid line: DOS; dotted curve: $3d$ DOS; dash-dotted curve: $\langle b \rangle^2 \times 3d$ DOS, dashed curve, $2p$ DOS. The weighting factor $\langle b \rangle^2$ in the $3d$ projected DOS is appropriate for calculating the d component in photoemission spectra.

extra weight being found in a $d^9 \rightarrow d^{10}$ satellite to be expected near E_1 , i.e., to the left of the band illustrated in Fig. 6 (such a satellite was explicitly calculated in Ref. 32). In Fig. 7 the d weight at the Fermi level (dotted curve) is plotted versus doping and is seen to be about 45% at 25% doping. This fraction is similar to the fractional d weight deduced from photoemission experiments.⁶

In contrast to the d weight, NMR data has been used to derive the fraction of spin of $3d$ character.³³ On the

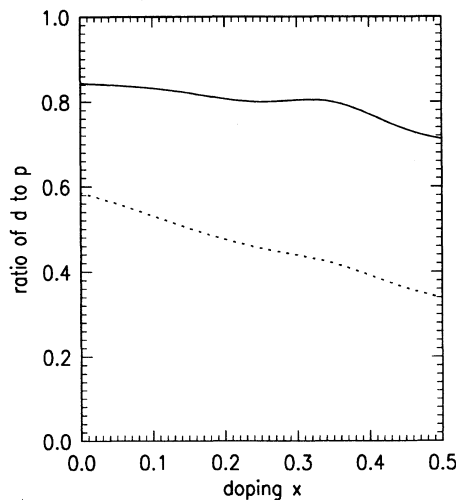


FIG. 7. Ratio of weights of copper to oxygen in states at Fermi level vs doping x . Dashed curve: spin degree of freedom (appropriate in NMR); dotted curve: charge degree of freedom (appropriate in photoemission spectra). From mean-field calculation based on 2:2:1:2 model of Table I.

basis of uniform susceptibility, this would be obtainable from the fraction of $3d$ in the Fermi level DOS, without correcting for the $\langle b \rangle^2$ factor. This is illustrated in Fig. 7 by the dashed curve. The values are seen to be about 80%, compared to an experimental number³³ of 70%.

In Fig. 8 the amount of oxygen character to the left of the Fermi level in Fig. 5, i.e., the oxygen-hole number in the system, is plotted versus doping. The amount of oxygen holes is seen to increase almost directly as the added holes. The meaning of this is plain: at all dopings there is some admixture of holes into copper states, leading to some 20% probability of Cu being in the $3d^{10}$ state, but that almost all doped holes go into the oxygen states. This seems to be a physically correct picture, and the illustrated data follows it very closely.

Also in Fig. 8 we illustrate the mean-field plasma sum rule, the details of the calculation being given in Appendix A. The method differs somewhat from that of Grilli, Kotliar, and Millis.²³ The experimental plasma frequency tends to increase more rapidly with doping than the theoretical prediction (the agreement would be a lot better for the isotropic Anderson-lattice model, as discussed in Appendix A). It appears that at the mean-field level the screening out of the current from the $3d$ to the $2p$ states is significantly less well described than is the screening of the static $3d$ charge fluctuations, which, as shown in the foregoing paragraph, seemed to be described quantitatively in mean field. This difficulty may be linked to that in describing the insulator in mean-field (leading- N) theory, and is probably due to the presence of Hartree-Fock (HF)-like elements in the ground state. In HF, characteristic of conventional spin rather than the $SU(N)$ of mean-field theory, there is a link between the 2 of $SU(2)$ and the 2 in the bipartite lattice, leading in the insulating limit to the antiferromagnetic state.

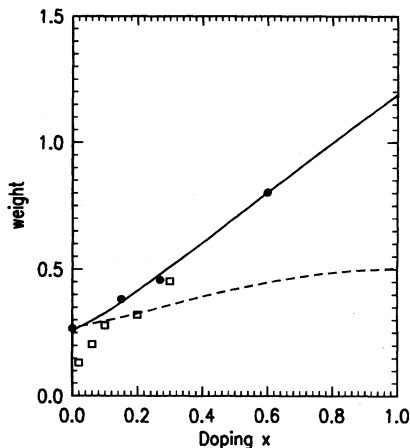


FIG. 8. Solid curve: number of oxygen holes vs doping; solid circles: data of Himpsel *et al.*³⁷ (arbitrary normalization); dashed curve: plasmon sum rule in mean-field approximation, expressed as square of plasma frequency in units of 0.1 eV^2 (see Appendix A); open squares: data of Tajima *et al.*³⁴ and Schlesinger *et al.*⁵ (cutoff 1.5 eV). 1:2:3 doping assumed 0.3. Theoretical curves from mean-field calculation based on 2:2:1:2 model of Table I.

We see then that the mean-field solution, simple though it is, has certain characteristic features that arise from the energy-level diagram of Fig. 1, which imposes a large gap Δ for charge fluctuations of the d states, but readily permits fluctuations in d spin. Among these characteristic features are that the added holes go into the oxygen, that photoemission will find oxygen states slightly predominant at the Fermi level, but that NMR will find the Cu states wholly predominant at the Fermi level. These expectations are just what is observed. The latter measurement reflects the existence of a $3d$ resonance at the Fermi level, which is seen in much reduced strength in photoemission because the $3d$ strength is moved away into the d^9-d^{10} satellite.³²

Turning to the approach to the metal-insulator transition, we illustrate in Fig. 9 the expectation value of the boson squared, $\langle b \rangle^2$, which controls the dd hopping amplitude and thus the bandwidth of the band in Fig. 6. Thus it is effectively inverse band mass. For our parameters, which are as realistic as possible, the quantity is nearly constant for hole doping. But, for larger values of $|E_1|$, corresponding to overall heavier masses, $\langle b \rangle^2$, and thus the inverse band mass, vanishes at zero doping.

As several authors have pointed out, the second type of scenario provides a bonus in explaining the metal-insulator transition, which will come about through the vanishing of the kinetic energy of the carriers as doping goes to zero. But trends such as the susceptibility of the 2:1:4 material (Fig. 2) go quite the wrong way for this picture, in which the susceptibility should diverge at the low doping end. Moreover, the masses seem not to be heavy enough overall to be located in the region where mass goes to infinity at zero doping. Therefore we think that the mean-field theory, in the realistic region, has a problem with the metal-insulator transition. One way out, which we recently proposed,³⁵ is that there may be a first order phase boundary interceding somewhere below 10% doping. Other ideas are that the true mass does, in a better approximation, go to infinity, but in a very abrupt

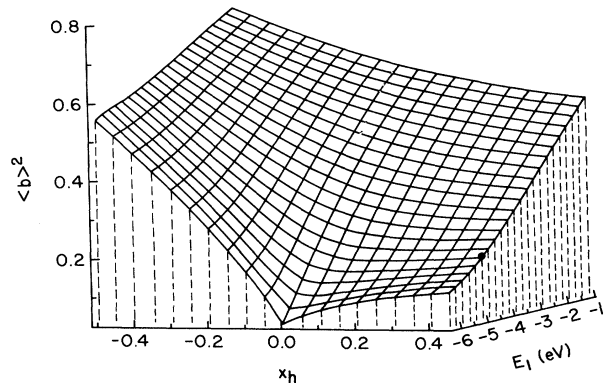


FIG. 9. Plot of $\langle b \rangle^2$ vs doping x_h and E_1 for mean-field treatment of the 2:2:1:2 model of Table I. The quantity $\langle b \rangle^2$ is approximately a measure of the mass renormalization m/m^* . Note important distinction between curves that go to infinite mass at zero doping, and those that go to finite mass.

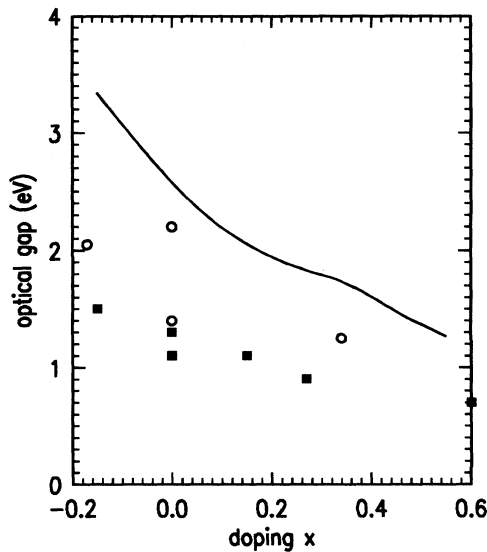


FIG. 10. Plot of optical gap vs doping x . Curve: 2:2:1:2 model, mean field; open circles: optical data from Tokura;³⁶ solid squares: data of Himpsel *et al.*³⁷

manner below, say 5% doping. The metal-insulator transition, like the superconductivity, seems to form a fertile subject for future work.

As a final topic for this section, we consider the comparison between the optical gap defined as the difference between the bottom of the oxygen (hole) band and the Fermi level, and some experimental data on the 2:1:4 material. This is done in Fig. 10. The comparison comes out quite well as regards the overall trend and the general magnitude of the gap. The optical data shows a discontinuity in the gap as a function of doping trend as the insulator is crossed, a discontinuity not seen in the technique of Ref. 37, or in the mean-field curve which constrains the system to metallic character.

IV. CONCLUSION

Mean field, then, explains with one parameter a significant amount of data, a situation which has already become clear for some time, though in this paper we have tried to extend the comparisons a little beyond those in the literature, and at the same time aim at a quantitative description of the system. Of particular interest is the picture of the high- T_c systems that emerges from this type of study, a picture that we return to shortly.

The comparisons of mean field with the data so far have shown that a successful understanding can be achieved of the paramagnetic susceptibility and specific heat, the energy dispersion seen in photoemission, the shape and topology of the Fermi surface, the relative weights of copper and oxygen both in NMR and photo-

emission spectroscopies, the observed energy gaps in the p - and n -type materials, and the scaling with doping of the number of oxygen holes. The energy gap and plasma sum rule show the deviations from smooth metallic behavior as a function of doping at half filling associated with the development of the insulating gap.

These positive results come about because in a simple way the slave-boson mean-field approximation can handle the spinlike nature of the Cu $3d$ orbitals, due to suppression of $3d$ charge fluctuations by the large U and the substantial charge transfer gap, together with the nearly noninteracting behavior of the oxygen holes (the $3d$ current seems less adequately suppressed, however). Mean field achieves these results without separating spin and charge, and in the context of a Luttinger Fermi surface, which contains both the spinlike Cu $3d$ holes and the weakly interacting oxygen $2p$ holes. It is then important for the success of these comparisons that the high- T_c systems are close to Fermi-liquid behavior, though apparently not exactly in the Fermi-liquid state ("marginal behavior").

An important aspect of our mean-field modeling is what it tells us about the high- T_c systems. Light is thrown on several issues. First of all, how does mass behave with doping? There has been discussion^{22,33} that the mass might diverge at zero doping, providing a free explanation of the metal-insulator transition. However, our calculation, along with the data, suggests that it does not, rather the insulating phase is interjected into an otherwise smooth variation of mass from negative to positive doping. The interjection of the insulating phase shows up in the optical measurements of the gap in Fig. 10 as a discontinuity in the gap as doping crosses through zero. It is not clear whether the insulating phase becomes stable near half-filling in a first-order sense,³⁵ or whether some other description is appropriate. The gap itself, between the top of the (electron) oxygen bands, and the Fermi-level, is found to decrease with doping. But it does not vanish, which means that the system can really be described by bands belonging just to the CuO_2 planes over a wide range of doping.

A more surprising conclusion, found initially from running slave-boson mean-field programs with the accurate NRL band structure parametrizations, and then from the data that confirm these theoretical assumptions, is that in the high- T_c systems the Fermi level lies remarkably close to the Van Hove singularity in the DOS. Because the systems are quasi-two-dimensional, this singularity is close to a logarithmic divergence. Direct experimental evidence for this situation is seen in angle-averaged photoemission data,⁶ which may be compared with a linear combination of the dashed and dash-dotted curves in Fig. 6 (section above hole Fermi level). The data⁶ shows the peak at the Fermi level expected from Fig. 6. A consequence of this situation is that we can reconcile the light effective masses seen in angle-resolved photoemission with the large DOS implied by all the measurements of paramagnetic susceptibility and specific-heat jump included in Table III, without introducing large Fermi-liquid parameters.

Why the foregoing situation should occur in high- T_c

systems cannot be fully discussed in this paper. However, several authors, such as Dzyaloshinskii,³⁸ Friedel,³⁹ Labbe *et al.*,⁴⁰ and Tsuei,¹¹ have attributed the high T_c 's in the high- T_c materials to the Van Hove singularity, and if some scenario along their lines is correct, then no coincidence is involved.

With this understanding gained, we can be less surprised by results such as the quasilinear behavior of the imaginary part of the self energy (inverse lifetime broadening of a quasiparticle) with energy from the Fermi level. This is observed over a relatively coarse energy scale of order 0.05–0.3 eV in ir and angle-resolved photoemission measurements. Now if the systems were interacting Fermi systems with a nearly constant DOS, the $\text{Im}\Sigma(\epsilon)$ would go as $\epsilon^2 \ln \epsilon$. But the presence of the logarithmic singularity lying within say 10–30 meV of the Fermi level is expected to significantly modify this behavior in the sense of slowing the energy dependence. For example suppose that in calculating the self-energy due to electron-electron scattering, we angle average the response function just as the phonon response function is angle-averaged in Eliashberg theory. Then if the Fermi energy lies close to the logarithmic Van Hove singularity, the lifetime broadening scales as $\epsilon^2 \ln(\epsilon)^3$ a behavior found to be indistinguishable from linear with ϵ over a wide range. More detailed calculations confirm this assertion based on angle-averaging.⁴¹

In the higher- T_c materials it seems likely that the Fermi level is pinned within \sim one to two times T_c of the Van Hove singularity. The actual doping level required to produce this situation depends on band-structure parameters and varies from material to material, and is optimally high to escape from the effects of the metal-insulator transition. Note that although the system in a sense contains a half-filled Hubbard resonance, the large dopant concentration prevents Fermi surface nesting, and hence the tendency towards antiferromagnetism of the half-filled Hubbard model is held in check. Nevertheless the bands run almost parallel to the Fermi level in a region of \mathbf{k} space around the saddle point of $E(\mathbf{k})$, leading to more phase space for scattering than is normal in 2D Fermi liquids. Such systems never get to a region where the DOS is analytic about the Fermi level, and might be termed van Hove liquids. In this case the resistivity should also show the quasilinear function $T^2 \ln(T)^3$ as discussed above for the self energy. Maybe also the anomalous lifetime of the copper nuclear spin can find an explanation in this context.

We must expect to have to go beyond the mean-field (leading N) approximation in order to explain features of the data that depend on the current, such as the plasma frequency and Hall coefficient, even though in certain models such as the isotropic Anderson-lattice and Kondo-lattice models a full enumeration of the leading- N diagrams should lead to the physically correct results.

ACKNOWLEDGMENTS

It is a pleasure to acknowledge the contribution of many colleagues, among whom are R. T. Collins, J. E. Demuth, G. B. Kotliar, H. R. Krishnamurthy, A. J. Millis, T. Penney, M. Ronay, and Z. Schlesinger. We are

most grateful for the assistance of D. A. Papaconstantopoulos with band-structure parametrization, and to F. J. Himpfel and to Y. Gao for the use of unpublished data.

APPENDIX

The plasmon sum rule is calculated starting from the 2:2:1:2 Hamiltonian in the basis of Bloch states formed from the d and p orbitals

$$\mathcal{H} = \sum_{k,\alpha,\beta,\sigma} h_{\alpha\beta}(k) C_{k\alpha\sigma}^\dagger C_{k\beta\sigma} + U \sum_{(i,\alpha)=d} C_{i\alpha\sigma}^\dagger C_{i\alpha\sigma} C_{i\alpha-\sigma}^\dagger C_{i\alpha-\sigma} \quad (\text{A1})$$

Here i =site, k =Bloch wave vector, α =orbital. The sum rule on the spectral density can be computed from (A1) as

$$N/m = -q^{-2} \langle [\rho_{-q}, [\rho_q, \mathcal{H}]] \rangle, \quad (\text{A2})$$

where the density operator is

$$\rho_q = \sum_{k,\alpha,\sigma} C_{k\alpha\sigma}^\dagger C_{k+q\alpha\sigma} \quad (\text{A3})$$

and N is the number of holes, and m defines the mass in the spectral density sum rule.

Calculating (A2), we obtain

$$N/m = \frac{1}{2} \sum_{k,\alpha,\beta,\sigma} [\nabla^2 h_{\alpha\beta}(k)] \langle C_{k\alpha\sigma}^\dagger C_{k\beta\sigma} \rangle. \quad (\text{A4})$$

In order to estimate a spectral density sum appropriate over a low frequency regime of order the characteristic energy scale ϵ_F of the system, (A4) is evaluated in mean field, replacing the operator D_σ by $\langle b \rangle D_\sigma$ wherever it occurs.

An analytic solution to the sum rule for N/m in (A4) can be given for the simple case of the isotropic Anderson-lattice model of the first reference of Ref. 16; $N/m = n_0^h/m_0$, where n_0 is the number of oxygen holes and the separated oxygen bands disperse as $\epsilon_k = k^2/m_0$. The current is in this model entirely associated with the oxygen states, and the trend of ω_p^2 versus doping would follow that of the n_0^h curve in Fig. 8. In the Kondo-lattice limit the result simplifies further to $N/m = x/m_0$; i.e., the plasmon frequency scales exactly as the doping.

To simplify (A4) in the case of the 3-band model, we drop the small O-O-NNN and Cu-Cu NN matrix elements in Table I. Then using the mean-field expression for $\langle b \rangle$, (A4) becomes

$$\frac{N}{m} a^2 = \frac{1}{4} \{ \lambda \langle b \rangle^2 - \langle H_0 \rangle \} \quad (\text{A5})$$

in the notation of Eq. (1); a is the Cu-Cu distance. The first term in (A5) comes from d - p hopping, while the second (positive) terms comes the oxygen degree of freedom and is analogous to the n_0^h/m_0 term for the isotropic Anderson-lattice model. The first term is not negligible. At zero doping the first and second terms are 0.15, 0.23 going to 0.22, 0.49 at $x=1$. Because of the presence of the d - p hopping term, and the slower dependence on

doping of the oxygen energy in (A5) relative to the n_0^h of the isotropic Anderson-lattice model, the sum rule for the three-band model (A5) increases rather slowly with doping (see Fig. 8).

Expression of N/m in terms of a plasma frequency requires introduction of a background dielectric constant ϵ_0 . Then $\omega_p^2 = 4\pi e^2 \epsilon_0^{-1} c^{-1} N/ma^2$, where c is the interplanar spacing. ϵ_0 is taken to be 4.

- ¹P. W. Anderson, *Science* **235**, 1196 (1987); P. W. Anderson, G. Baskaran, Z. Zhou, and T. Hsu, *Phys. Rev. Lett.* **58**, 2790 (1987); G. Baskaran and P. W. Anderson, *Phys. Rev. B* **37**, 580 (1988).
- ²H. Eskes and G. A. Sawatzky, *Phys. Rev. Lett.* **61**, 1415 (1988); H. Eskes, L. H. Tjeng, and G. A. Sawatzky, *Phys. Rev. B* **41**, 288 (1990).
- ³B. H. Brandow (private communication).
- ⁴M. S. Hybertson, M. Schluter, and N. E. Christensen, *Phys. Rev. B* **39**, 9028 (1989); A. K. McMahan, R. M. Martin, and S. Satpathy, *ibid.* **38**, 6650 (1988).
- ⁵Z. Schlesinger, R. T. Collins, F. Holtzberg, C. Field, S. H. Blanton, U. Welp, G. W. Crabtree, Y. Fang, and J. Z. Liu, *Phys. Rev. Lett.* **65**, 801 (1990).
- ⁶C. G. Olson, R. Liu, D. W. Lynch, R. S. List, A. J. Arko, B. W. Veal, Y. C. Chang, P. Z. Jiang, and A. B. Paulikas, *Phys. Rev. B* **42**, 381 (1990).
- ⁷C. Hodges, H. Smith, and J. W. Wilkins, *Phys. Rev. B* **4**, 302 (1971).
- ⁸K. S. Bedell (unpublished).
- ⁹M. W. Shafer, T. Penney, B. L. Olson, R. L. Greene, and R. H. Koch, *Phys. Rev. B* **39**, 2914 (1989).
- ¹⁰S. Uchida, H. Takagi, Y. Tokura, N. Koshihara, and T. Arima, in *Strong Coupling and Superconductivity*, edited by H. Fukuyama, S. Maekawa, and A. P. Malozemoff (Springer-Verlag, Heidelberg, 1989), p. 194.
- ¹¹C. C. Tsuei, A. Gupta, and G. Koren, *Physica C* **161**, 415 (1989); C. C. Tsuei, in *Proceedings of the 3rd Bar-Ilan Conference on Frontiers in Condensed Matter Physics, Israel, 1990* [*Physica A* (to be published)].
- ¹²C. M. Varma, P. B. Littlewood, S. Schmitt-Rink, E. Abrahams, and A. E. Ruckenstein, *Phys. Rev. Lett.* **63**, 1996 (1989).
- ¹³N. Nagaosa and P. A. Lee, *Phys. Rev. Lett.* **64**, 2450 (1990); L. P. Ioffe and D. P. Wiegmann, *Phys. Rev. Lett.* **65**, 653 (1990); M. Grilli, B. G. Kotliar, and A. J. Millis, *Phys. Rev. B* **42**, 329 (1990).
- ¹⁴K. A. Müller (unpublished).
- ¹⁵M. Imada and Y. Hatsugai, *J. Phys. Soc. Jpn.* **58**, 3752 (1989); M. Frick, P. C. Pattnaik, I. Morgenstern, D. M. Newns, and W. von der Linden, *Phys. Rev. B* **42**, 2665 (1990).
- ¹⁶D. M. Newns, M. Rasolt, and P. C. Pattnaik, *Phys. Rev. B* **38**, 6513 (1988); D. M. Newns, P. C. Pattnaik, M. Rasolt, and D. A. Papaconstantopoulos, *ibid.* **38**, 7033 (1988).
- ¹⁷P. B. Littlewood, C. M. Varma, S. Schmitt-Rink, and E. Abrahams, *Phys. Rev. B* **39**, 12371 (1989).
- ¹⁸D. L. Cox, M. Jarrell, C. Jayaprakash, H. R. Krishnamurthy, and J. Deisz, *Phys. Rev. Lett.* **62**, 2188 (1989).
- ¹⁹D. M. Newns and P. C. Pattnaik, in *Strong Coupling and Superconductivity*, edited by H. Fukuyama, S. Maekawa, and A. P. Malozemoff (Springer-Verlag, Heidelberg, 1989), p. 194.
- ²⁰M. J. de Weert, D. A. Papaconstantopoulos, and W. E. Pickett, *Phys. Rev. B* **39**, 4235 (1989); D. A. Papaconstantopoulos (private communication).
- ²¹M. S. Hybertson, M. Schluter, E. B. Stechel, and D. R. Jennison (unpublished); C. X. Chen, H. B. Schuttler, and A. J. Fedro, *Phys. Rev. B* **41**, 2581 (1990).
- ²²J. H. Kim, K. Levin, and A. Auerbach, *Phys. Rev. B* **39**, 11633 (1989); Q. Si, J. H. Kim, J. P. Lu, and K. Levin, *ibid.* **42**, 1033 (1990).
- ²³B. G. Kotliar and J. Liu, *Phys. Rev. Lett.* **61**, 1784 (1988); C. Castellani and B. G. Kotliar, *Phys. Rev. B* **39**, 2876 (1989); M. Grilli and B. G. Kotliar, *Phys. Rev. Lett.* **64**, 1170 (1990); Grilli, Kotliar, and Millis, Ref. 13.
- ²⁴F. Mehran, T. R. McGuire, and G. V. Chandrasekhar, *Phys. Rev. B* **41**, 11583 (1990).
- ²⁵A. Junod, D. Eckert, T. Graf, G. Triscone, and J. Muller, *Physica C* (to be published).
- ²⁶Y. Gao, J. E. Crow, G. H. Myer, P. Schlottman, and J. Schwegler (unpublished).
- ²⁷K. Kitazawa *et al.*, *Japan J. Appl. Phys. Pt. 2* **26**, L751 (1987).
- ²⁸T. Kawagoe, T. Mizoguchi, K. Kanoda, T. Takahashi, M. Hasumi, and S. Kagoshima, *J. Phys. Soc. Japan* **57**, 2272 (1988); Y. Yamaguchi, M. Tokumoto, S. Waki, Y. Nakagawa, and Y. Kimura, *J. Phys. Soc. Jpn.* **58**, 2256 (1989).
- ²⁹J. B. Torrance, A. Bezing, A. I. Nazzari, T. C. Huang, S. S. P. Parkin, D. J. Keane, S. J. LaPlaca, P. M. Horn, and G. A. Held, *Phys. Rev. B* **40**, 8872 (1989).
- ³⁰D. B. Mitzi, L. W. Lombardo, A. Kapitulnik, S. S. Lederman, and R. D. Jacowitz, *Phys. Rev. B* **41**, 6564 (1990).
- ³¹In the mean-field 32-band calculation of Ref. 16 it was found that the Fermi level hit the bottom of the oxygen valence-band system at above 15% doping, making the simple planar model inapplicable beyond this point. The shift in level with increasing doping, which undoubtedly exists (see Fig. 10) and comes from hole-hole repulsion, is exaggerated in mean field because this neglects the attraction of the doping centers that accompany the added holes. This attraction tends to compensate the hole-hole repulsion, since a given hole sees as many attractive centers as it does other holes. However, the attractive centers are out of plane and thus should undercompensate the repulsion.
- ³²P. C. Pattnaik and D. M. Newns, *Phys. Rev. B* **41**, 880 (1990); Sá de Melo and S. Doniach, *ibid.* **41**, 6633 (1990); H. Eskes and G. A. Sawatzky (private communication).
- ³³M. Takigawa, P. C. Hammond, R. H. Heffner, and Z. Fisk, *Phys. Rev. Lett.* **63**, 1865 (1989).
- ³⁴S. Tajima, S. Tanaka, T. Ido, and S. Uchida, in *Proceedings of the Second International Symposium on Superconductivity, Tsukuba, Japan* (Springer-Verlag, Heidelberg, 1990).
- ³⁵H. R. Krishnamurthy, P. C. Pattnaik, and D. M. Newns (unpublished).
- ³⁶A. Fujimori, Y. Tokura, H. Eisaki, H. Takagi, S. Uchida, and M. Sato, *Phys. Rev. B* **40**, 4303 (1989); Y. Tokura (private communication).
- ³⁷A. Santoni, M. Ronay, L. J. Terminello, G. V. Chandrasekhar, M. W. Shafer, Y. Hidecha, and F. J. Himpsel (private communication).
- ³⁸J. E. Dzyaloshinskii, *Pis'ma Zh. Eksp. Teor. Fiz.* **46**, 97 (1987) [*Sov. Phys. JETP Lett.* **46**, 118 (1987)]; *Zh. Eksp. Toer. Fiz.* **93**, 206 (1987) [*Sov. Phys. JETP* **66**, 848 (1987)].
- ³⁹J. Labbe and J. Bok, *Europhys. Lett.* **3**, 1225 (1987).
- ⁴⁰J. Friedel, *J. Phys. (Paris)* **48**, 1787 (1987); *ibid.* **49**, 1435 (1988).
- ⁴¹P. C. Pattnaik, D. M. Newns, and C. C. Tsuei (unpublished).